Draft tube flow phenomena across the bulb turbine hill chart

P Duquesne[1], **R Fraser**[1], **Y Maciel**[1], **V Aeschlimann**[1], **C Deschênes**[1]
Hydraulic Machine LAboratory (LAMH), Department of Mechanical Engineering,
Laval University, Pavillon Adrien-Pouliot, 1065 avenue de la medicine,
Québec G1V 0A6, Canada

E-mail: pierre.duquesne.1@ulaval.ca

Abstract. In the framework of the BulbT project launched by the Consortium on Hydraulic Machines and the LAMH (Hydraulic Machine Laboratory of Laval University) in 2011, an intensive campaign to identify flow phenomena in the draft tube of a model bulb turbine has been done. A special focus was put on the draft tube component since it has a particular importance for recuperation in low head turbines. Particular operating points were chosen to analyse flow phenomena in this component. For each of these operating points, power, efficiency and pressure were measured following the IEC 60193 standard. Visualizations, unsteady wall pressure and efficiency measurements were performed in this component. The unsteady wall pressure was monitored at seven locations in the draft tube. The frequency content of each pressure signal was analyzed in order to characterize the flow phenomena across the efficiency hill chart. Visualizations were recorded with a high speed camera using tufts and cavitation bubbles as markers. The predominant detected phenomena were mapped and categorized in relation to the efficiency hill charts obtained for three runner blade openings. At partial load, the vortex rope was detected and characterized. An inflection in the partial load efficiency curves was found to be related to complex vortex rope instabilities. For overload conditions, the efficiency curves present a sharp drop after the best efficiency point, corresponding to an inflection on the power curves. This break off is more severe towards the highest blade openings. It is correlated to a flow separation at the wall of the draft tube. Also, due to the separation occurring in these conditions, a hysteresis effect was observed on the efficiency curves.

1. Introduction

With the increase of the energy cost and unavailability of accessible high head sites in developed countries, exploitation of low head sites become profitable. For these sites, bulb turbines often have advantages over other types, like lower construction costs, large operating ranges and straight diffusers. Bulb turbine technologies reached maturity since the first industrial implementations in 1962 at “La Rance” and “Pierre Benitte” in France [1, 2, 3], but a detailed experimental study of flows in bulbs is not yet available. In comparison, other types of turbines were intensively studied, for example Francis turbine [4], a Kaplan turbine at the Turbine99 workshops [5] and more recently a propeller turbine in the AxialT project [6]. This is why the Consortium in Hydraulic Machines, headed by the Laval University hydraulic machines laboratory (LAMH), has set up the BulbT project.

A particularly critical part of low head turbines is the draft tube, where the recuperation has the same order of magnitude than the water head. The recuperation coefficient represents the conversion of kinetic energy in static pressure energy. For example, the BulbT turbine recuperation in the diffuser is estimated at 42% of the total head for the best efficiency point found with the 30° runner blade

angle. It is therefore important to minimise the energy losses in the draft tube, to maximize recuperation and to increase the turbine global efficiency. In this context, the BulbT project is strongly focussed on draft tube flow phenomena.

This paper first introduces the engineering performances measured for the BulbT model as represented on efficiency hill charts. Unsteady wall pressure measurements were recorded in the draft tube for each operating point and analysed. Then cavitation and wool-tuft visualisations were performed at some selected points. These systematic measurements allowed identifying flow phenomena producing losses and mapping their location on the efficiency hill charts. A hysteresis effect is presented in the last section of this paper.

2. Experimental setup

A section view of the BulbT turbine currently under investigation at the LAMH is shown in figure 1. The main specificity of this model is certainly the immerged eddy current brake designed to dissipate the energy and to control the runner speed. No mechanical transmission like in most bulb model test benches is necessary [7]. The bulb part containing the brake is immerged in the entrance channel and maintained by two piers. The distributor is composed of 16 guide vanes that control the flow rate. The runner has four adjustable blades. The draft tube is divided in two major parts: the acrylic conical part and the transition part. The conical part has a half opening angle of 10.25°. The transition part, which is circular at the entrance and rectangular at the outlet, is symmetric between right and left, and asymmetric between top and bottom: the bottom wall diverges and the upper wall is horizontal. An overview of the referential used in this paper is also represented in figure 1, the z direction being axial, the y vertical and the x transversal.

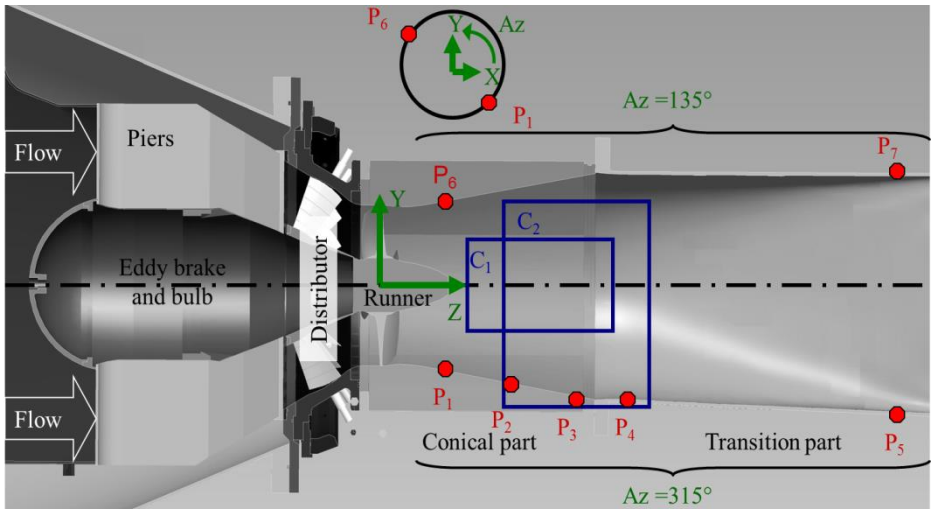

Figure 1. Overview of BulbT model. Visualisation zones are represented by blue box noted C_1 and C_2. Wall pressure sensors are identified with P_i symbols and red circles. Az corresponds to the azimuthal positions of the probes.

The test bench follows recommendation of IEC 60193 norm [8]. The model rotation velocity and torque are directly measured inside the bulb and transmitted by a wireless technology. Unless otherwise noted, acquisitions of 90 second at 1 kHz were performed for each operating points. Results are provided using the following unit coefficients:

$$N_{11} = \frac{N\ D_{ref}}{\sqrt{H}}\ ;\ Q_{11} = \frac{Q}{\sqrt{H}}\ ;\ P_{11} = \frac{P}{D_{ref}^{\ 2}\ H^{3/2}} \qquad (1)$$

where N is the model rotation velocity (rpm), H the net water head (m), Q the flow rate (m³/s), P the extracted mechanical power (W) and D_{ref} the runner shroud diameter (m).
The efficiency η is defined by:

$$\eta = \frac{P}{\rho \cdot g \cdot H \cdot Q} \tag{2}$$

where ρ is the water density (kg/m³) and g the gravitational constant (m/s²).

In this study, three blade angles (BA) are investigated: 15°, 22.5° and 30°. The best efficiency point has been measured at 22.5°. Efficiency hill charts are presented in figures 8, 9 and 10 respectively for these three blade openings, based on 266, 206 and 171 operating points.

The pressure sensors made-up for this study are Unisensor ships mounted at the end of a 4 mm outlet diameter probes. Sensor alimentations and signal conditionings are delivered by Meiri 520-AS conditioners having a maximal frequency range of 20 kHz. The acquisition is ensured by a National Instrument PCI-6036E acquisition card board and the Labview environment. The calibration of the acquisition chain and sensors revealed a linear and Gaussian behavior. A total accuracy of 0.15 % on the pressure range of 200 kPa has been calculated. Seven of these sensors were flush mounted on the walls. Their small diameters ensure a good hydraulic continuity in accordance with the IEC 60193 norm [8]. They are localised and numbered in figure 1. To estimate the draft tube recuperation, two sensors (P_1 and P_6) were located at draft tube intlet and two others (P_5 and P_7) at the outlet. Pressure signals from sensors P_1, P_2, P_3 and P_4 were devoted to frequency spectrum analysis. Pressure measurements were taken for each operating points at 200 Hz with 10 000 samples.

Visualisations were performed to confirm and correlate flow phenomena with the pressure signals. A high speed camera was used to capture cavitation bubbles at 500 fps during 10s in the zone designated as C_1 in figure 1. This camera was also used at 300 fps during 23s to detect flow separations in the C_2 zone made visible by wool-tuft indicators glued on walls.

3. Criteria for flow phenomena identification

3.1. Draft tube losses

The water head recuperation in the draft tube depends on the pressure and velocity fields. The draft tube recuperation corresponds to the conversion of kinetic energy into static pressure energy that can be captured by the runner. The available kinetic energy normalized by the total head available can be estimated by:

$$E_k = \left(\left(\frac{Q}{A_1} \right)^2 - \left(\frac{Q}{A_2} \right)^2 \right) \frac{1}{2 \cdot g \cdot H} \tag{3}$$

Where A_1 and A_2 are respectively the draft tube inlet and outlet areas.
The static pressure energy recovery normalized by the total head available can be estimated from pressure measurements. Using pressure taps identified in figure 1, it becomes:

$$E_P = \left(\frac{P_5 + P_7}{2} \right) - \left(\frac{P_1 + P_6}{2} \right) \frac{1}{\rho \cdot g \cdot H} \tag{4}$$

Due to the importance of head recuperation compared to the total head available, the diffuser has a direct and important impact on efficiency and power extraction. The draft tube design is however a compromise between short length with high opening angle to limit civil costs and generation of losses in the diffuser. In figure 2, three curves are represented for fixed N_{11} and blade angle: the efficiency curve in red, the theoretical head recuperation using eq. (3) in black and the experimental head recuperation using eq. (4) in blue. In this example, the best efficiency point corresponds to the maximal recuperation of 32% of the total head. The gap between the theoretical and experimental

recuperations, hatched in green, is attributed to draft tube losses. In the complete efficiency hill-charts (figure 8, 9 and 10), we define zones where draft-tube losses are not significant respecting the following criteria:

$$E_K - E_P < 1\% \quad (5)$$

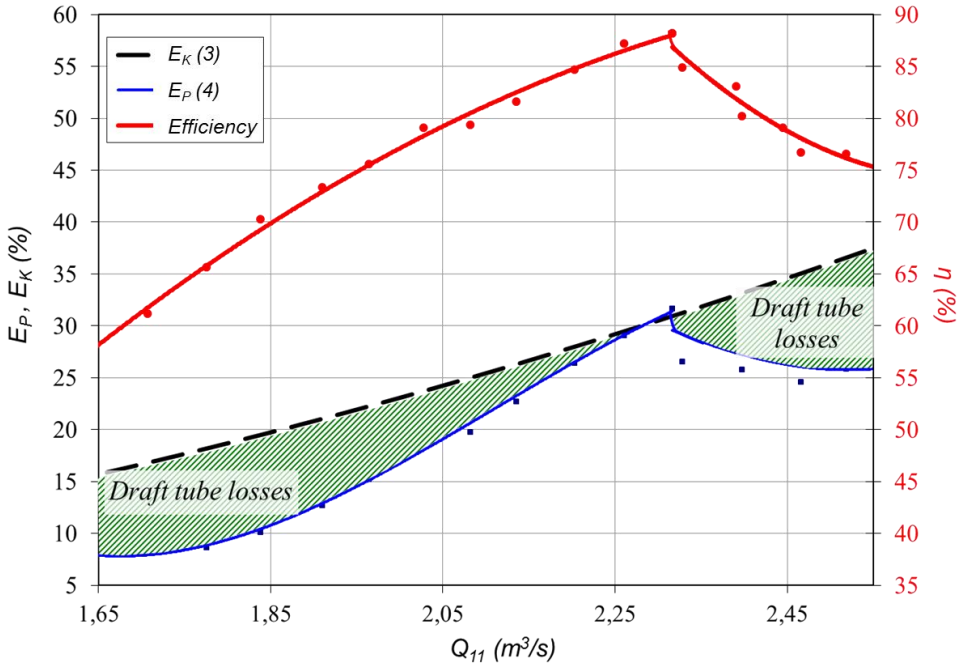

Figure 2. Efficiency and water head recuperation for blade angle 22.5° (BA=22.5°) and N_{11}= 170 rpm. Draft tube losses are represented by hatched zones.

3.2. Vortex rope at partial load condition

The mean velocity fields downstream the turbine runner at part load can be represented by three vortices [9]. The inner vortex is co-rotating with the hub and counter flowing per reference to the hub axis. A counter rotating and co-flowing vortex is found around this inner vortex. And finally the rest of the flow circulated in a rigid body rotation with a constant debiting axial velocity. The vortex rope is generated at the hub and develops itself at the interface between the inner vortex and the counter rotating vortex. Several vortex ropes have been observed on different turbine types, often with cavitation visualization [10], [11] and [12]. A particular frequency generally between 1/5 *N* and 1/3 *N* characterizes for them. Escudier [13] associates vortex ropes to non-optimal velocity repartition and bad energy extraction. The draft tube recuperation is affected, the inner vortex and the counter rotating vortex acting as hydraulic obstacles that reduce the recuperation area. This aspect is predominant in bulb turbine draft tubes.

To detect the vortex rope, a spectral analysis of the pressure sensor P1 signal was done. The frequencies with the largest amplitudes were extracted for partial load conditions. For the same N_{11}, each blade angle had different vortex rope frequencies relative to *N*. As an example, a spectral analysis at partial load conditions for the three studied blade angles and specific Q_{11} and N_{11} is represented in figure 3. One can see that the vortex rope frequencies and amplitudes increase with the blade opening. The observed pics correspond to the vortex rope frequencies and their harmonics. Also, vortex frequency variations were noticed for fixed blade angles (not shown): the rope accelerated with decreasing Q_{11}, particularly for Q_{11} ranging from 0.8 to 1.8 m^3/s, and a similar effect was observed with decreasing N_{11}.

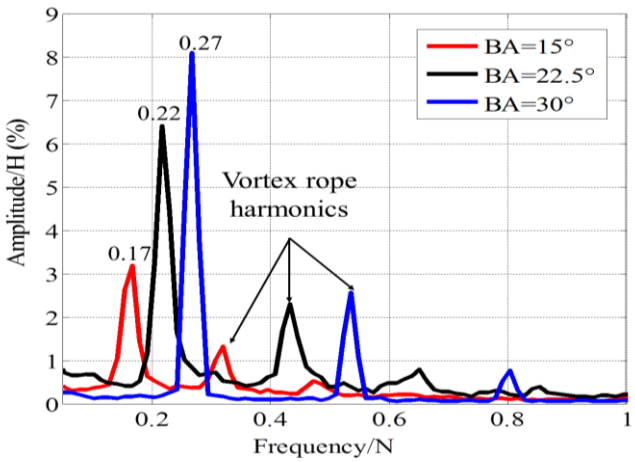

Figure 3. Spectral analysis of sensor 1 at N_{11}=160 rpm and Q_{11}= 1, 1.3 and 1.7 m^3/s for respectively BA=15°, 22.5° and 30°.

For blades angles at 15°, 22.5° and 30°, the predominant frequencies were respectively 0.19 *N*, 0.25 *N* and 0.29 *N*. In order to represent the area of the hill charts where the vortex ropes can be found, an interval of ±0.05 *N* was defined. In the complete efficiency hill charts of figures 8, 9 and 10, the zones where vortex ropes were detected are hatched in red. Therefore, all points in these areas present vortex ropes with a predominant frequency ±0.05 *N*. Arrows in these figures indicate frequency evolutions at constant N_{11} and the local mean frequencies are indicated in red.

Highest frequency vortex ropes correspond to low Q_{11} and N_{11}, reaching nearly half the runner frequency as marked with red zones in figures 8, 9 and 10. These vortex ropes are not cavitating but sudden frequency variations suggest another flow pattern still to be investigated.

The efficiency curves from part load to BEP show inflexions. Figure 4 shows an example for blade opening 22.5° at three different N_{11}. Following the scientific literature that reports vortex breakdown for a Francis turbine [14], some type of vortex break down was suspected here too. Cavitation observations performed on BulbT for blade openings 22.5° and 30° allowed to correlate the inflections in the efficiency curves at part load with vortex rope breakdowns. Figure 5 gives a time evolution example of an observed vortex breakdown. In this case, the cavitating rope is a small axial filament enhanced in red dash lines. Its pattern is not regular and is subject to spiral breakdown [15], as shown in the second picture of figure 5. In figures 8, 9 and 10, points with inflections are encircled with black lines.

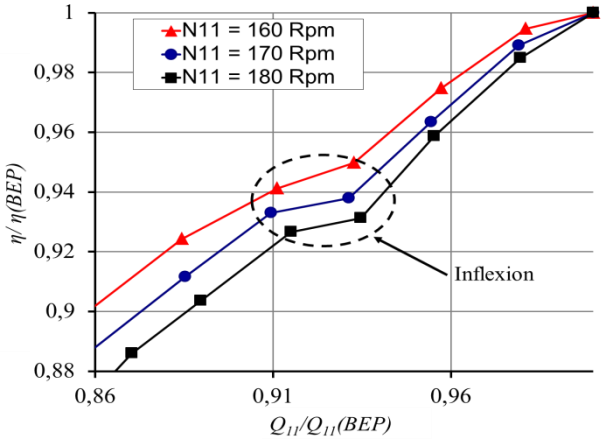

Figure 4. Efficiency curve at partial load for BA= 22.5° for N_{11} = 160, 170 and 180 rpm.

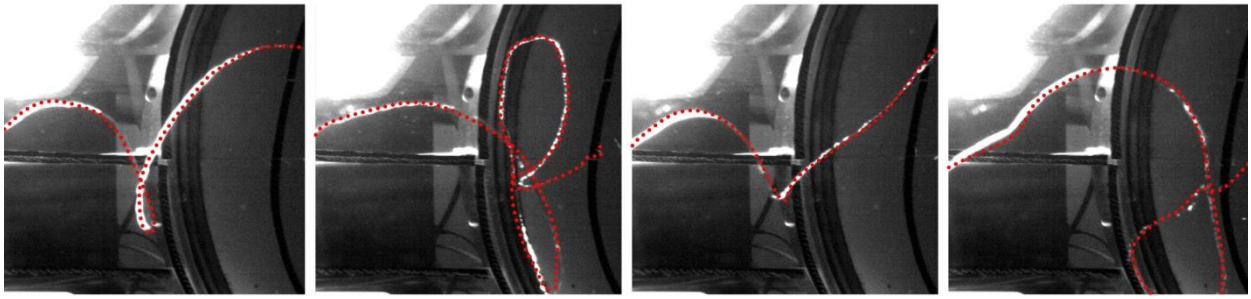

Figure 5. Pictures at each 0.2s. N_{11}=170 rpm, and BA=22.5°: Vortex breakdown.

3.3. Draft tube flow separation at overload condition

A break off occurs in the BulbT performances at overload conditions. As can be seen in figure 6 for N_{11} = 170 rpm and increasing Q_{11}, a sharp drop appears in the efficiency and power curves. This break off is more prominent for high blade angle openings and high N_{11}. Flow separation induces stagnation and backflow regions at the diffuser wall acting as hydraulic obstacles that reduce the effective diffuser section. Since the pressure recuperation is linked with the cross section (eq. (3)), reducing the section alters the pressure recuperation and finally reduces efficiency and power. Separation has been already identified on a Francis model showing similar break off in [16]. Moreover, figure 6 tends to endorse the known fact that the main parameter susceptible to trig flow separations in a diffuser is the flow rate.

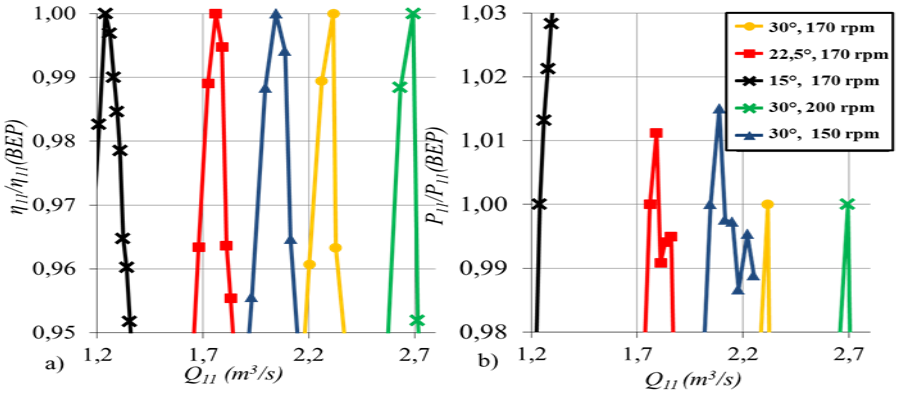

Figure 6. Break off on a) efficiency and b) power for N_{11}=170 rpm at different blade angle and at different N_{11} for BA=30°. Guide vanes gap between two measures is 2°.

Wool-tuft visualisations at N_{11} =170 rpm for two different blade angles (22.5° and 30°) confirmed the presence of flow separation. A preliminary broad investigation revealed flow separation at the end of the conical diffuser part and in the transition part. A systematic investigation allowed focusing on this zone, which is identified by C_2 in figure 1. Results show that the flow separation is correlated to the break off apparition as suspected. At constant N_{11}, the separation starts when the operation point is close to the local BEP. It begins in the left downside of the transition section and expands rapidly in the conical part with the opening of the guide vanes. The flow separation structure appears to be complex, turbulent and presents different time and spatial scales.

Following these qualitative visualisations, unsteady wall pressure measurements were performed. Pressure sensors P_2, P_3 and P_4 were located in the separation zone observed with tufts. FFT analysis of their pressure signals showed no peak at particular frequencies, with or without flow separation. But a bulge on low frequencies was detected, corresponding to different time and spatial scales of the flow separation structure. Figure 7 represents spectral analysis of the three sensors signals at an operating point without flow separation (figure 7a) and with separation (figure 7b).

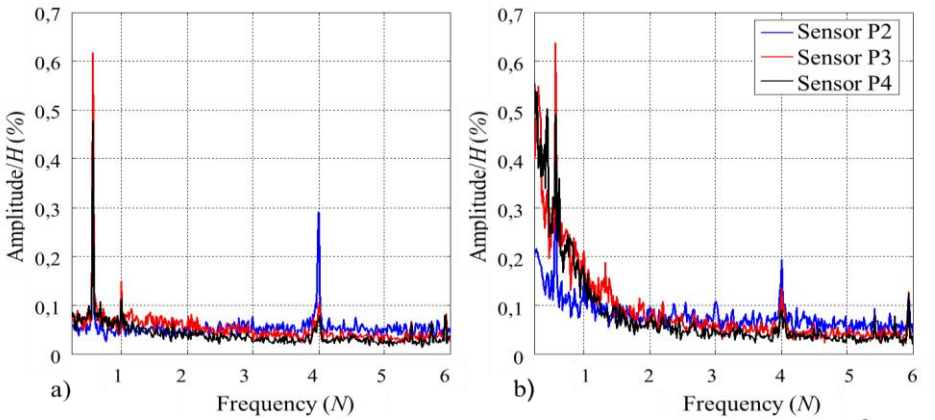

Figure 7. Low frequency analysis at N_{11} = 170 rpm, BA=30° a) Q_{11}= 2.3 m^3/s without flow separation. b) Q_{11}= 2.4 m^3/s with separation.

Figure 7b shows a low frequency bulge correlated to the flow separation. The generation of low-frequency fluctuations in an unsteady pressure signal has already been reported for separation zones in the backward-facing step, for example [17]. Based on this observation, the bulge can be used as an indicator of flow separation in the draft tube. Pressure signals of sensors P_2, P_3 and P_4 were used to define a criterion at overload conditions for the BulbT case:

$$\frac{\sum Amplitude(\mathrm{F} \leq \mathrm{N})}{\sum Amplitude} > 25\% \qquad (6)$$

The nominator of (6) corresponds to the sum of the signal amplitudes up to the rotation speed *N*, while the denominator corresponds to the sum of all amplitudes of the spectral analysis. This criterion was used to delimit the separation zones shown in blue in figures 8, 9 and 10.

4. Mapping of flow phenomena on the efficiency hill

The efficiency hill charts for three blade openings are presented in figures 8, 9 and 10, with the different zones of specific flow phenomena defined in the previous sections.

The “losses not significant” zones identified in green represent areas where losses in the draft tube have a low impact according to eq. (5). For all blade openings, this zone is located near the best efficiency of each N_{11} constant curve. At low blade angles, 15° for example (figure 8), flow phenomena have smaller intensities and generate smaller losses than at higher angles. The zone without predominant losses is also larger but the pressure recuperation in the diffuser is inferior to 16% of *H*. Since the recuperation is proportional to the flow rate, as can be seen in eq. (3), recuperation becomes more important for the higher 22.5° and 30° blade opening angles (figures 9 and 10). The zones without predominant losses are narrower around the best efficiency points for these, but the recuperation reaches respectively 30% and 42%, allowing more power extraction.

A vortex rope pattern classification in three elements was introduced in section 3.2: the classic vortex rope, vortex rope at higher frequency and vortex rope with vortex breakdown. The vortex ropes presenting a classical pattern have a frequency which increases with the blade opening, from 0.19 *N* at 15° blade opening to 0.29 *N* at 30°. The predominant vortex rope at 15° has a very low velocity of 0.19 *N*. The high speed vortex rope, nearing 0.5 *N*, covers a larger zone for the 15° blade opening. This zone is located at partial discharge where the efficiency is low. At higher blade angles, the high speed vortex rope zone is smaller and the difference between high speed and low speed becomes smaller. Inside the range Q_{11} = 0.8 to 1.8 m^3/s, the rope frequency accelerates with decreasing Q_{11} and N_{11}.Vortex rope instabilities with axial filament breakdowns are observed at part load and represented with black lines in figure 8 to 10. Finally, vortex ropes disappear near the BEP.

The draft tube flow separation zones in figures 8 to 10 are located where the discharge is large and where the hydraulic power is supposed to be maximal. This has a particular importance from an industrial point of view since the power extraction unfortunately drops in this zone and should be investigated further. The flow separation zones are tridimensional and fluctuate in size, position and time. However, these fluctuations do not appear periodic. At low blade angle, the flow separation zone is small and its impact on the power is moderate, the power keeps increasing with the discharge. At higher blade angle, however, the separation zone is larger and it expends with the flow rate. For 30° opening, the flow separation zone is closer to the BEP and it impacts the power output.

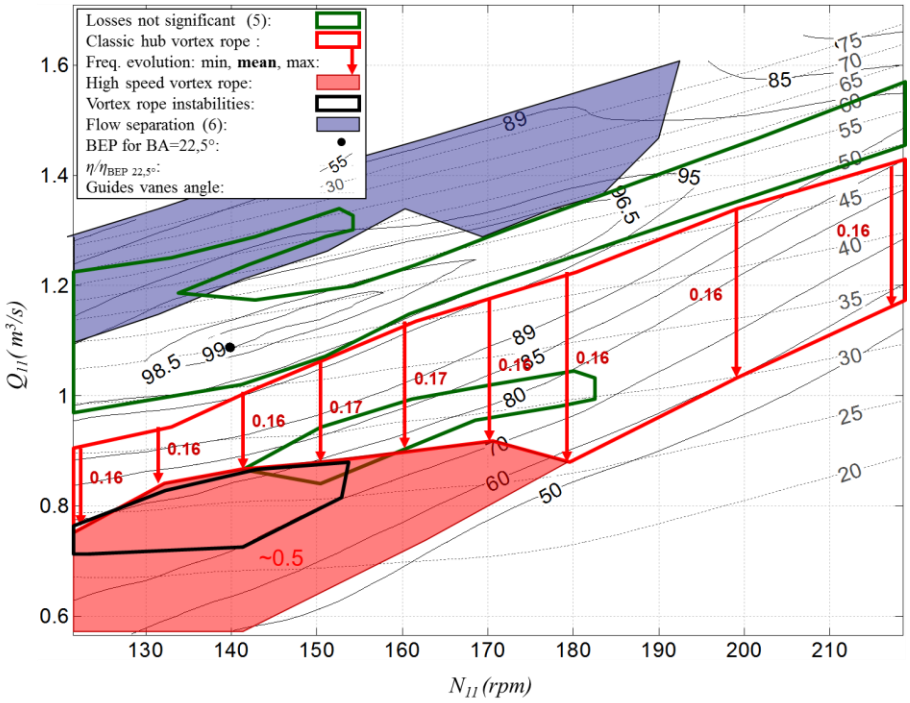

Figure 8. Efficiency hill for BA=15°.

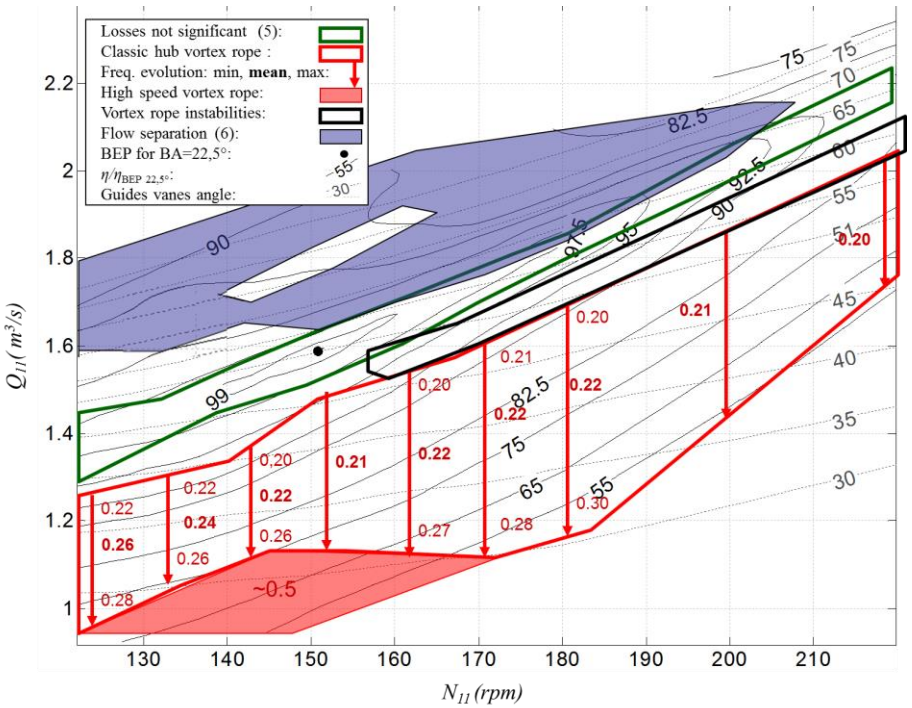

Figure 9. Efficiency hill for BA=22.5°.

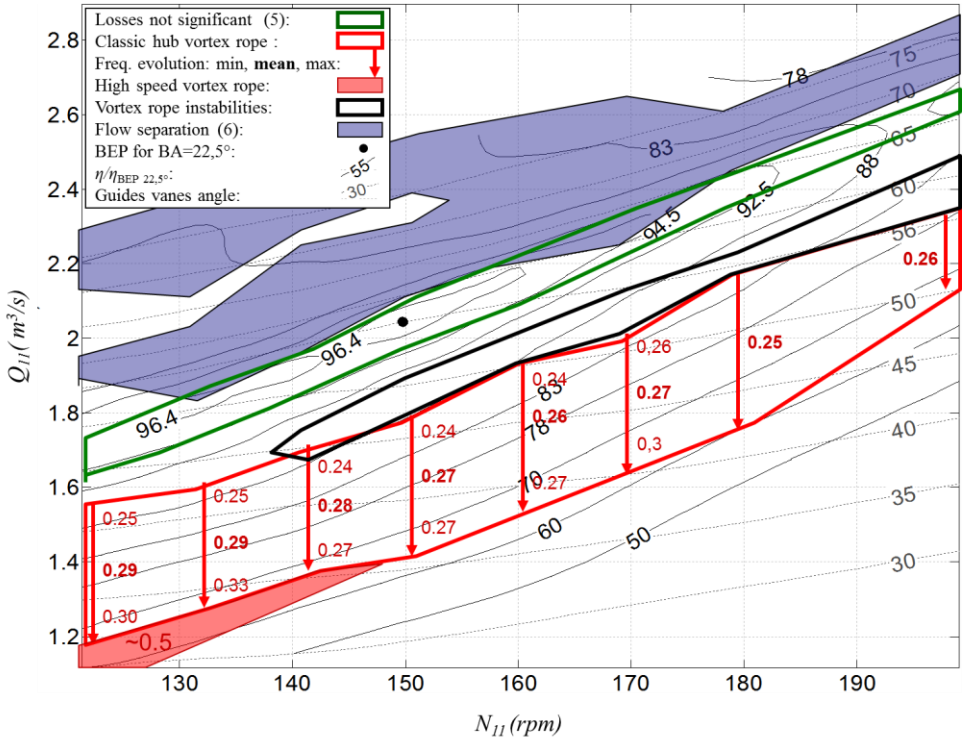

Figure 10. Efficiency hill for BA=30°.

5. Hysteresis effect

Some difficulties to repeat overload conditions were encountered when a large unsteady flow separation occurs in the draft tube. This effect has been observed as well on a Francis turbine and a bulb turbine [18, 19]. So additional tests were performed to investigate the suspected hysteresis effect in this hill chart zone. At constant N_{11}, model performances have been measured both in opening the guide vanes and in closing them. This process has been repeated two times. During these runs, each operation condition was measured up to 15 minutes at 1 kHz to ensure convergence. Figure 11 presents a close up of the efficiency hill chart in the break off zone at N_{11} =170 rpm. The opening run is represented with the blue curve and the closing run with the red curve. The repetition runs are represented by pale blue and dark red points. One can notice for example a drop of the efficiency up to 1.5% for the same 64.5° guide vane angle.

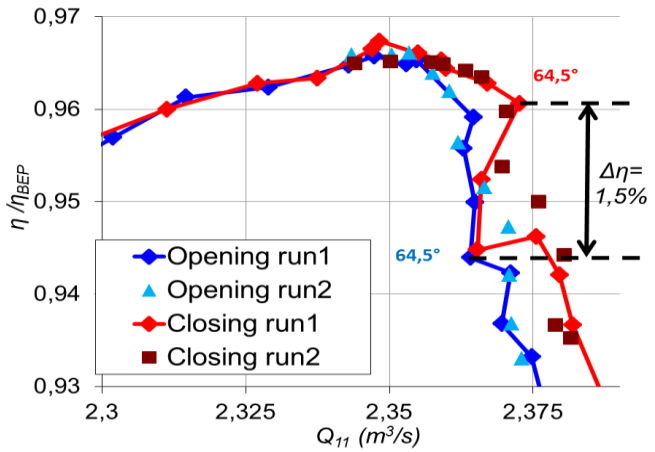

Figure 11. Influence of flow history on efficiency curve with N_{11}=170 rpm BA= 30°.

In the same hill chart zone, it was impossible to systematically reach a target operating point by moving the guide vanes from a random initial position. Furthermore, a larger dispersion was noticed when choosing a target operating point with important flow phenomena in the diffuser. This situation can be hypothetically explained by the inertial nonlinear term in the Navier-Stokes equations, which allows the flow behaviour to be led by the flow history. A classic example of this historic effect is the Couette flow between two independently rotating cylinders [20]. The flow separation in this flow configuration is greatly affected by the previous flow condition. Flow separation history effects have also been observed in other fluid applications, for example in different stall angles associated with increasing or decreasing the attack angle of a wing profile. To ensure sufficient repeatability to study the flow in the beak off zone of the bulb turbine, a strict start-up sequence protocol was defined to reach specific operating points. The guide vane angle is first set while there is no flow. Then, the main test rig pump is started with constant acceleration until the targeted flow rate is reached. While the runner rotation speed is obtained by a proportional-integral-derivative (PID) controller.

6. Conclusion

An experimental study of the BulbT model turbine was presented in this paper. The focus was put on the draft tube since this component produces important head recuperations in low head turbines. Strong hydraulic phenomena occurring in this part can lead to head-losses with serious impact on global performances. Different losses phenomena have been identified in the studied draft tube and mapped on the efficiency hill charts. The complete guide vane opening range was investigated for three angle openings of the runner blades. Specific criteria for the most common draft tube phenomena loses were defined and systematic detection tests were performed on a total of 643 operating conditions.

Visualizations, unsteady wall pressure measurements and engineering quantities have been acquired to detect major flow patterns. Three different behaviors of the vortex rope were observed at partial load. First, predominant classic vortex rope frequencies were identified through the pressure measurements at about 0.19 N, 0.25 N and 0.29 N respectively for the 15°, 22.5° and 30° blade openings. High speed vortex ropes have also been detected in the pressure signals. Finally vortex rope instabilities with axial filament breakdowns have been observed and correlated with efficiency inflection.

The most prominent flow phenomenon in the draft tube was flow separation leading to sharp power and efficiency break off at overload conditions. It was found that oscillations and turbulence associated with this flow separation generate low frequency bulges on the pressure signals, providing a sure way to detect them. The large flow separation in the draft tube also present brings hysteresis behavior linked to the previous operating conditions. This behavior led to define a special start up procedure to ensure measurement repeatability.

This study constitutes the preliminary investigation of the BulbT model. Further investigations are ongoing with a particular focus on the break off zone at blade angle 30° and N_{11} = 170 rpm.

Acknowledgement

The authors would like to thank the participants of the Consortium on Hydraulic Machines for their support and contribution to this research project: ALSTOM Renewable Power Canada Inc. , Andritz Hydro LTD, Hydro-Quebec, Laval University, NRCan, Voith Hydro Inc. Our gratitude goes as well to the Canadian Natural Sciences and Engineering Research Council who provided funding for this research.

References

[1] Casacci S 1973 Les groupes bulbes projets et perspective *La houille blanche* **2/3** 229-46
[2] Cazenave P 1997 L'utilisation des groupes bulbes dans l'aménagement de basse chute *La houille blanche* **3** 25-31

[3] Beslin M 1973 Idées actuelles sur la conception des groupes bulbes. Exemple de Caderousse *La houille blanche* **2/3** 201-14
[4] Chirag T, Cervantes M J, Gandhi B K, and Dahlhaug O G 2013 Experimental and numerical studies for a high head Francis turbine at several operating points *J. Fluids Eng.* **135**
[5] Gebart B R, Gustavsson L H, and Rolf K 1999 Report from Turbine-99 - Workshop on draft tube flow *Luleå University of Technology*
[6] Deschênes C, Ciocan G D, De Henau V, Flemming F, Huang J, Kollers M, Naime FA, Page M, Qian R and Vu T 2010 General overview of the AxialT Project: a partnership for low head turbine developments *Proc. of the 25th Symp. on Hydr. Mach. And Syst.*
[7] Fraser R, Vallée D, Jean Y and Deschênes C 2014 Eddy current brake for fully homologous bulb turbine model testing *Proc. of the 27th Symp. on Hydr. Mach. And Syst.*
[8] C.E.I. 1999 Norme internationale C.E.I. 60193: Turbines hydrauliques, pompes d'accumulation et pompes-turbines. Essais de réception sur modèle
[9] Susan-Resiga R, Ciocan G D, Anton I and Avellan F 2006 Analysis of the Swirling Flow Downstream a Francis Turbine Runner *J. Fluids Eng.* **128** 177-89
[10] Ciocan G D, Iliescu M, Vu T, Nennemann B and Avellan F 2007 Experimental study and numerical simulation of the FLINT draft tube rotating vortex *J. Fluids Eng.* **129** 146-58
[11] Houde S, Iliescu M, Fraser R, Lemay S, Ciocan G D and Deschênes C 2011 Experimental and numerical analysis of the cavitating part load vortex dynamics of low-head hydraulic turbines *Proc. of ASME-JSME-KSME Joint Fluids Engineering Conference* **2** 171-182
[12] Jonsson P P, Mulu B G and Cervantes M J, 2012 Experimental investigation of a Kaplan draft tube- Part II: Off-design conditions *Appl Energ*. **94** 71-83
[13] Escudier M, 1987 Confined Vortices in Flow Machinery *Annu. Rev. Fluid Mech*. **19** 27-52
[14] Susan-Resiga R, Muntean S, Hasmatuchi V, Anton I and Avellan F 2010 Analysis and Prevention of Vortex Breakdown in the Simplified Discharge Cone of a Francis Turbine *J. Fluids Eng*. **132(5)**
[15] Lucca-Negro O and O'Doherty T 2001 Vortex breakdown: a review *Prog Energy Combust* **27** 431-81
[16] Tridon S, Barre S, Ciocan G D, Leroy P and Ségoufin C 2010 Experimental investigation of draft tube flow instability *Proc. of the 25th Symp. on Hydr. Mach. And Syst.*
[17] Farabee T M and Casarella M J 1986 Measurements of Fluctuating Wall Pressure for Separated/Reattached Boundary Layer Flows *J. of Vib., Acoust. Stress and Reliable*. **108(3)** 301-07
[18] Tridon S, Barre S, Ciocan G D and Tomas L 2009 Experimental description of swirling flow downstream a Francis turbine runner and initialization of numerical simulations *Proc. of the 25th Symp. on Hydr. Mach. And Syst.*
[19] Ran H J, Luo X W, Chen Y L, Xu H Y and Farhat M 2012 Hysteresis phenomena in hydraulic measurement. *Proc. of the 26th Symp. on Hydr. Mach. And Syst.*
[20] Andereck C D, Liu S S and Swinney H L 1986 Flow regimes in a circular Couette system with independently rotating cylinders *J.Fluid Mech* **164** 155-183